KINEMATIC ANALYSIS OF TWO DEGREES-OF-FREEDOM PLANAR SEVEN-BAR MECHANISMS WITH PRISMATIC PAIRS

Mingquan Yang,* JunWang,* and Yizhe Huang*

Abstract

The two-degrees-of-freedom (DOF) planar seven-bar mechanism is a complicated mechanism because of its two closed kinematic chains and two input joints that lead to its motion's complexity. The majority of previous research in this area primarily focuses on the mechanism with only revolute pairs. Since the revolute pair only produces rotational motion, the need for translational movement is unaddressed. Translational motion created by a prismatic pair where the prismatic pair moves in the same direction at the same speed is needed in numerous mechanical structures. Therefore, kinematic analysis of the two-DOF planar seven-bar mechanisms with a prismatic pair and with two prismatic pairs is necessary. Paired with three-dimensional (3D) simulation, the method for the analysis is algebraic. Firstly, singularity curves, dead center positions, branches, and branch points of the two proposed mechanisms were identified via mathematical analysis; so was the rotational or translational displacement of each joint in each proposed mechanism. Secondly, the singularity configurations of the mechanisms at branch points were simulated and verified via the mechanisms' 3D models. Lastly, the sub-branches of each mechanism were identified mathematically and described by demonstrating different configurations of the mechanisms in different sub-branches via their 3D models.

Key Words

Prismatic pair, singularity curve, dead center position, branch, branch point, sub-branch

1. Introduction

In the research of planar mechanisms, the analysis of planar mechanisms' motion is crucial. Singularity curves, dead center positions, branch curves, branches, branch points, and sub-branches are the elements that affect the motion of a planar mechanism. A branch of a planar mechanism refers to the range of motion where the mechanism operates continuously with given parameters without being disassembled. The boundaries of a branch are called branch curves which are sections of the singularity curves also known as the collections of dead center positions, some of which are branch points. If a planar mechanism encounters a dead center position or branch point, the movement of the mechanism is impeded. Hence, dead center positions should be avoided. In this paper, a bar in a multi-bar mechanism refers to a link that has two or multiple kinematic pairs.

The most comprehensive research on planar single-loop mechanisms' mobility was the rotatability laws for N-bar kinematic chains [1]–[4] and the concept of joint rotation space (JRS) [5], which offer a series of methods to study single-loop planar and spherical mechanisms' motion. Since a multi-loop planar mechanism is formed by single loops, these methods are also applicable to the kinematic analysis of multi-loop planar mechanisms [6]–[8]. In addition, scholars across the world have proposed other methods to analyse multi-loop planar mechanisms' motion. Dou and Ting [9] developed a module approach for the branch identification of a large variety of multi-loop linkages. Wang *et al.* [10] studied the Stephenson six-bar mechanism's two closed kinematic chains with the discriminant method and obtained, dead center positions, branches, branch points, and sub-branches of the mechanism. Wang *et al.* [11] put forward the concept of the equivalent four-bar linkage, with which the singularity of single-degrees-of-freedom (DOF) multi-loop mechanisms was thoroughly studied. Wang and Ting [12] achieved automated mobility identification of a group of single-DOF planar eight-bar linkages. Plecnik and McCarthy [13] presented function generators that offered a direct solution to the kinematic synthesis equations of the Stephenson-III six-bar mechanism. Compared with single-DOF multi-loop planar mechanisms, a two-DOF two-loop planar mechanism requires two input joints to determine its configurations and has more complex motion. Wang *et al.* [14]–[16] put forward a theoretical

* Institute of Additive Manufacturing and Industrial Robotics, School of Mechanical Engineering, Hubei University of Technology, Wuhan, Hubei 430068, China; e-mail: mingquan yang@outlook.com; junwang@hbut.edu.cn
Corresponding author: Jun Wang

Recommended by Raffaele Di Gregorio
(DOI: 10.2316/J.2024.206-0903)

method based on the discriminate method that analyses the singularity, branches, and sub-branches of planar two-DOF seven-bar parallel linkages and manipulators. Wang *et al.* [17] introduced the concept of the equivalent five-bar linkage which can geometrically identify the dead center positions of two-DOF seven-bar planar mechanisms. Nie and Ding [18] proposed a method based on the graph theory and transmission angles to identify two-DOF planar parallel manipulators' dead center positions. multi-loop planar mechanisms with more than two DOF offer even more complex motion and greater potential for industrial application. Therefore, many scholars proposed different methods to study their motion characteristics. Wang *et al.* [19] analysed the dead center positions of a series of multi-DOF multi-loop planar mechanisms with a degeneration method. Liu *et al.* [20] proposed a methodology to identify branches, circuits, and movement range of complex Assur groups (AGs) and created a novel discriminant method for identifying singularity configurations of complex AGs.

The kinematics of other types of planar mechanisms with only revolute pairs have also been investigated. Some scholars proposed different methods to study the motion of planar mechanisms with joint clearances [21]–[23]. Based on planar four-link mechanisms, other scholars [24], [25] created manipulators of different purposes, generated desired output motion, and established control methods. Many scholars investigated the kinematics of planar parallel mechanisms with only revolute pairs [26]–[32], and invented devices based on them for practical industrial usages. Chen *et al.* [33] invented and investigated a new type of planar two-DOF remote center of motion mechanisms for minimally invasive surgeries.

Some researchers have focused on designing and analysing planar mechanisms with prismatic pairs to produce translational motion. Soh and Ying [34] designed a motion generation method of six-bar and eight-bar mechanisms with prismatic pairs which were employed in redesigning wheelchairs with multiple functions. Almestiri *et al.* [35] presented a trajectory generation method for closed-loop mechanisms with prismatic pairs and revolute pairs. Zou *et al.* [36] designed a three-DOF parallel manipulator without rotational capacity where planar revolute joints and prismatic joints were exclusively employed. Zarkandi [37] utilised the concept of instant centers to conduct the isotropy analysis of multi-DOF planar parallel mechanisms with prismatic joints. Helal *et al.* [38] introduced a generalised algorithm to generate all alternatives of planar N-bar kinematic chains with sliders. Dharanipragada and Chintada [39] successfully conducted the isomorphism test on kinematic chains with prismatic pairs with the split hamming string method. Kang and Kim [40] put forward a topology optimisation method to synthesise a planar linkage mechanism with prismatic pairs, whose input motion is converted into a desired output motion at the mechanism's end effector. Zhao *et al.* [41] investigated the forward velocity, displacement, and acceleration of planar four-bar and five-bar slider-crank linkages. Essomba and Phu [42] presented a 3-PRP (P and R represents the prismatic and revolute pairs, respectively) planar mechanism connected to a 3-PRS tripod mechanism to perform the bone reduction surgery. Gallant and Gosselin [43] identified a planar 3-RPR mechanism's unconstrained motion with the mechanism's joint clearances considered, and thereafter studied the mechanism's singularities. Jhuang *et al.* [44] presented a method to study a closed-loop four-link statically balanced mechanism that possesses two prismatic joints. Rodriguez-Gonzales *et al.* [45] demonstrated an approach with a branching identification procedure to synthesize planar RRPR linkages.

As per the abovementioned literature review, the essentiality of the translational motion produced by prismatic pairs in various mechanical structures is clearly presented. Nevertheless, research on the two-DOF seven-bar mechanism with prismatic pairs is rarely involved. Methods to acquire prismatic joints' precise translational displacements have rarely been proposed. Therefore, this paper, based on the aforementioned research, proposes the two-DOF seven-bar mechanisms with a prismatic pair and two prismatic pairs to produce translational movement. The method to identify the proposed mechanisms' motion characteristics is also put forward. The method divides the analysis of the two proposed mechanisms into four segments. In the first segment, the two-DOF planar five-bar mechanism is studied. The second segment concerns recognising the JRSs of the two five-bar kinematic chains in each proposed mechanism according to the analysis and results of the first segment; the singularity curves, dead center positions, branches, and branch points of the proposed mechanisms are identified via mathematical analysis. In the third segment, the precise displacement of each joint in each proposed mechanism at each branch point is obtained. The proposed mechanisms' 3D models simulate the proposed mechanisms' motion and are utilised to verify the displacement of each joint at each branch point. The proposed mechanisms' singularity configurations at branch points are obtained mathematically, and later presented as well as verified by the mechanisms' 3D models. The fourth segment illustrates the proposed mechanisms' sub-branches via mathematical analysis and the mechanisms' 3D models. With the mathematical analysis and 3D simulation, each proposed mechanism's range of motion can be attained and the motion deficiencies of the mechanisms can be directly observed.

2. The Discriminant Method to Identify the Two-DOF Five-Bar Mechanism's Singularity Configurations

The schematic diagram of the two-DOF five-bar mechanism is described in Fig. 1(a); the 3D model of the five-bar mechanism is shown in Fig. 1(b).

In Fig. 1(a), every single solid line with an arrow, which symbolises a vector, represents a link. Link AE is the fixed link; the input joints are D and E. Since $\vec{AB} + \vec{BC} = \vec{AE} + \vec{ED} + \vec{DC}$, (1) can be derived according to the Euler loop equation based on Euler's formula.

$$a_2 e^{i\theta_2} + a_3 e^{i\theta_3} = a_1 e^{i\alpha} + a_5 e^{i\theta_5} + a_4 e^{i\theta_4} \tag{1}$$

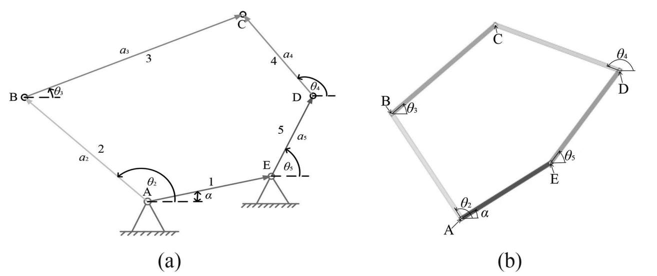

Figure 1. (a) The schematic diagram; (b) the 3D model of the two-DOF planar five-bar mechanism.

Equation (1) can be converted into (2) and (3).

$$a_3 \cos\theta_3 = a_1 \cos\alpha + a_5 \cos\theta_5 + a_4 \cos\theta_4 - a_2 \cos\theta_2 \quad (2)$$
$$a_3 \sin\theta_3 = a_1 \sin\alpha + a_5 \sin\theta_5 + a_4 \sin\theta_4 - a_2 \sin\theta_2 \quad (3)$$

By eliminating θ_3, (4) and (5) can be acquired.

$$\begin{aligned}&(a_1 \cos\alpha + a_5 \cos\theta_5 + a_4 \cos\theta_4 - a_2 \cos\theta_2)^2\\ &\quad+(a_1 \sin\alpha + a_5 \sin\theta_5 + a_4 \sin\theta_4 - a_2 \sin\theta_2)^2 = {a_3}^2 \quad (4)\\ &{a_1}^2 + {a_2}^2 - {a_3}^2 + {a_4}^2 + {a_5}^2 + 2a_1a_5\cos(\theta_5-\alpha)\\ &\quad+2a_1a_4\cos(\theta_4-\alpha) + 2a_4a_5\cos(\theta_4-\theta_5)\\ &\quad-2(a_2a_4\sin\theta_4 + a_2a_5\sin\theta_5 + a_1a_2\sin\alpha)\sin\theta_2\\ &\quad-2(a_2a_4\cos\theta_4 + a_2a_5\cos\theta_5 + a_1a_2\cos\alpha)\cos\theta_2 = 0 \quad (5)\end{aligned}$$

With X_2 equallingtan $\frac{\theta_2}{2}$, $\sin\theta_2$ equals $\frac{2X_2}{1+X_2^2}$; $\cos\theta_2$ equals $\frac{1-X_2^2}{1+X_2^2}$. Therefore, (5) can be converted into (6).

$$A_2{X_2}^2 + B_2X_2 + C_2 = 0 \quad (6)$$

where

$$\begin{aligned}A_2 &= {a_1}^2 + {a_2}^2 - {a_3}^2 + {a_4}^2 + {a_5}^2 + 2a_1a_5\cos(\theta_5-\alpha)\\ &\quad+2a_1a_4\cos(\theta_4-\alpha) + 2a_4a_5\cos(\theta_4-\theta_5)\\ &\quad+2(a_2a_4\cos\theta_4 + a_2a_5\cos\theta_5 + a_1a_2\cos\alpha)\\ B_2 &= -4(a_2a_4\sin\theta_4 + a_2a_5\sin\theta_5 + a_1a_2\sin\alpha)\\ C_2 &= {a_1}^2 + {a_2}^2 - {a_3}^2 + {a_4}^2 + {a_5}^2 + 2a_1a_5\cos(\theta_5-\alpha)\\ &\quad+2a_1a_4\cos(\theta_4-\alpha) + 2a_4a_5\cos(\theta_4-\theta_5)\\ &\quad-2(a_2a_4\cos\theta_4 + a_2a_5\cos\theta_5 + a_1a_2\cos\alpha).\end{aligned}$$

Equation (7) describes the condition that (6) needs to satisfy to have roots.

$$\Delta_2 = {B_2}^2 - 4A_2C_2 = 4D_1D_2 \geq 0 \quad (7)$$

where

$$\begin{aligned}D_1 &= 2a_2\sqrt{{a_1}^2 + {a_4}^2 + {a_5}^2 + 2a_1a_5\cos(\theta_5-\alpha)}\\ &\qquad\overline{+2a_1a_4\cos(\theta_4-\alpha) + 2a_4a_5\cos(\theta_4-\theta_5)}\\ &\qquad+[{a_1}^2 + {a_2}^2 - {a_3}^2 + {a_4}^2 + {a_5}^2\\ &\qquad+2a_1a_5\cos(\theta_5-\alpha) + 2a_1a_4\cos(\theta_4-\alpha)\\ &\qquad+2a_4a_5\cos(\theta_4-\theta_5)]\end{aligned}$$

Table 1
The Dimensions for the Two-DOF Five-Bar Mechanism

a_1	a_2	a_3	a_4	a_5	α
5	6	6.5	6.3	5.5	30°

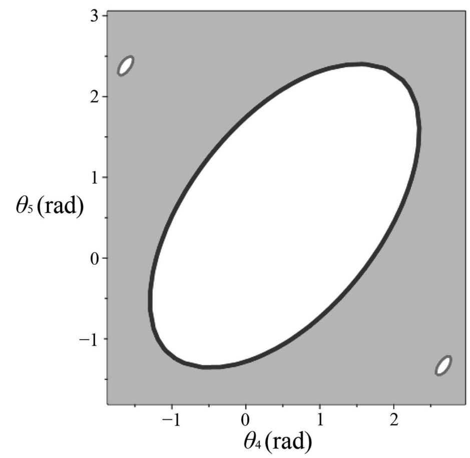

Figure 2. The JRS of the planar five-bar mechanism.

$$\begin{aligned}D_2 &= 2a_2\sqrt{{a_1}^2 + {a_4}^2 + {a_5}^2 + 2a_1a_5\cos(\theta_5-\alpha)}\\ &\qquad\overline{+2a_1a_4\cos(\theta_4-\alpha) + 2a_4a_5\cos(\theta_4-\theta_5)}\\ &\qquad-[{a_1}^2 + {a_2}^2 - {a_3}^2 + {a_4}^2 + {a_5}^2\\ &\qquad+2a_1a_5\cos(\theta_5-\alpha) + 2a_1a_4\cos(\theta_4-\alpha)\\ &\qquad+2a_4a_5\cos(\theta_4-\theta_5)].\end{aligned}$$

Equation (8) is employed to attain the value of θ_2 given that A_2 does not equal 0.

$$X_2 = \frac{-B_2 \pm \sqrt{\Delta_2}}{2A_2} \quad (8)$$

The dimensions for the proposed five-bar mechanism are enumerated in Table 1.

The JRS of the proposed five-bar mechanism is described in Fig. 2.

In Fig. 2, the two red and blue singularity curves are, respectively, obtained via D_1 and D_2 equalling 0; the shaded area is the JRS of the mechanism whose boundaries are the red and blue curves. With D_1 and D_2 equalling 0, the values of θ_4 and θ_5 were acquired; the value of θ_2 was obtained via (8); the value of θ_3 was obtained via (2) or (3). The values of θ_2, θ_3, θ_4, and θ_5 at dead center positions are enumerated in Table 2.

The values of θ_3 and θ_4 in dead center positions 1 and 2 are, respectively, on the red curve in the lower right corner and the blue curve in Fig. 2. The singularity configurations of the two dead center positions are displayed in Fig. 3(a) and (b).

According to Fig. 3(a) and (b), when D_1 or D_2 equals 0, links AB and BC coincide completely or form one single line without overlapping. In conclusion, with θ_4 and θ_5 being the two input angles, the three passive joints A, B, and C become collinear in singularity configurations.

Table 2
The Values of θ_2, θ_3, θ_4, and θ_5 at Dead Center Positions (D_1=0)

Joints	θ_2	θ_3	θ_4	θ_5
Dead center position 1	27.362°	−152.638°	154.699°	−80.355°
Dead center position 2	19.171°	19.171°	57.296°	−42.226°

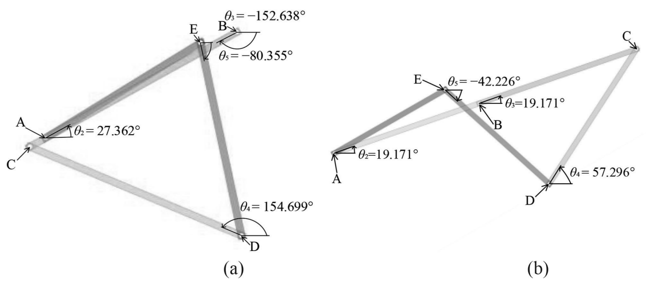

Figure 3. The planar five-bar mechanism at dead center positions: (a) 1 and (b) 2.

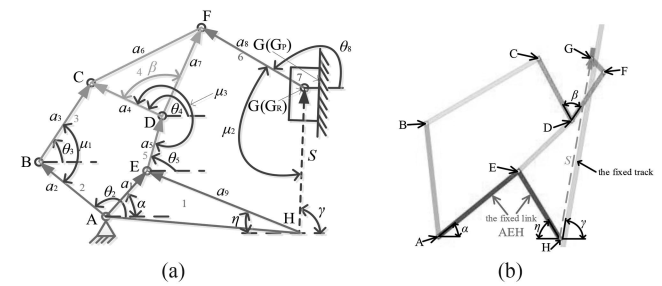

Figure 4. (a) The schematic diagram and (b) the 3D model of the planar two-DOF seven-bar mechanism with a prismatic pair.

3. Kinematic Analysis of the Two-DOF Planar Seven-bar Mechanism with a Prismatic Pair

3.1 The Establishment of the Euler Loop Equation Based on Euler's Formula

Figure 4(a) describes the schematic diagram of a planar two-DOF seven-bar mechanism with a prismatic pair; Fig. 4(b) shows the 3D model of the mechanism.

In Fig. 4(a), the rectangular slider G contains a prismatic pair G_P. The revolute pair on the slider is G_R. The revolute pairs also include A, B, C, D, E, and F; a_i represents the length of a specific link or a link's side and θ_i represents the displacement of a specific revolute joint. The triangular link CDF has two sides CD and DF, which are at an angle of β degrees. Each solid line with an arrow is a link or a side of a link in the mechanism represented by a vector; the dotted line with an arrow $\overrightarrow{HG}$, whose scalar value equals S, is also a vector that represents the translational motion of prismatic joint G. The sides, AE and EH, of the triangular link AEH are, respectively, at α and η degrees with the horizontal line; $\overrightarrow{HG}$ and the horizontal line are at an angle of γ degrees. With D and E designated as the two input joints and link AEH as the fixed link, the Euler loop equations based on Euler's formula are employed to describe the two five-bar kinematic chains of the mechanism.

In the five-bar kinematic chain ABCDE, as $\overrightarrow{AB}+\overrightarrow{BC} = \overrightarrow{AE}+\overrightarrow{ED}+\overrightarrow{DC}$, (9) can be derived.

$$a_2e^{i\theta_2} + a_3e^{i\theta_3} = a_4e^{i\theta_4} + a_1e^{i\alpha} + a_5e^{i\theta_5} \tag{9}$$

In the five-bar kinematic chain HEDFG, as $\overrightarrow{HE}+\overrightarrow{ED}+\overrightarrow{DF} = \overrightarrow{HG}+\overrightarrow{GF}$, (10) can be derived.

$$a_9e^{i(\pi-\eta)} + a_5e^{i\theta_5} + a_7e^{i(\theta_4-\beta)} = Se^{i\gamma} + a_8e^{i\theta_8} \tag{10}$$

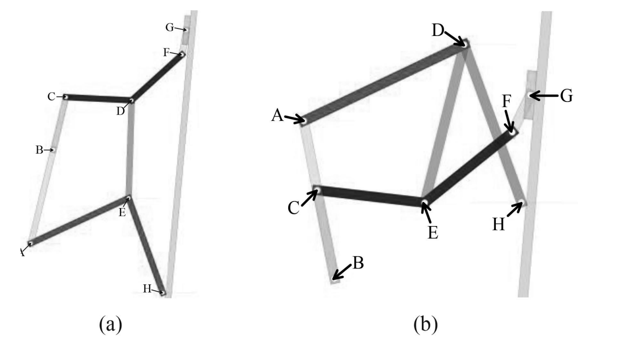

Figure 5. Links AB and the bar BC form (a) one single straight line without overlapping; (b) completely coincide.

According to the results of Section 2, the Euler loop equations for the two singularity configurations of ABCDE are described in (11) and (12).

Links AB and BC form one single straight line, as is shown in Fig. 5(a).

$$\begin{aligned}(a_2+a_3)e^{i\theta_2} &= a_4e^{i\theta_4} + a_1e^{i\alpha} + a_5e^{i\theta_5}\\ (a_2+a_3)\cos\theta_2 &= a_4\cos\theta_4 + a_1\cos\alpha + a_5\cos\theta_5\\ (a_2+a_3)\sin\theta_2 &= a_4\sin\theta_4 + a_1\sin\alpha + a_5\sin\theta_5\end{aligned} \tag{11}$$

Links AB and BC completely coincide where $\theta_3 = \theta_2 + \pi$, as is shown in Fig. 5(b).

$$\begin{aligned}a_2e^{i\theta_2} + a_3e^{i(\theta_2+\pi)} &= a_4e^{i\theta_4} + a_1e^{i\alpha} + a_5e^{i\theta_5}\\ (a_2-a_3)\cos\theta_2 &= a_4\cos\theta_4 + a_1\cos\alpha + a_5\cos\theta_5\\ (a_2-a_3)\sin\theta_2 &= a_4\sin\theta_4 + a_1\sin\alpha + a_5\sin\theta_5\end{aligned} \tag{12}$$

Equations (13) and (14) are obtained by eliminating θ_3 from (11) and (12), respectively.

$$\begin{aligned}&(a_4\cos\theta_4 + a_1\cos\alpha + a_5\cos\theta_5)^2\\ &\quad+(a_4\sin\theta_4 + a_1\sin\alpha + a_5\sin\theta_5)^2 = (a_2+a_3)^2\end{aligned} \tag{13}$$

$$(a_4 \cos\theta_4 + a_1 \cos\alpha + a_5 \cos\theta_5)^2 + (a_4 \sin\theta_4 + a_1 \sin\alpha + a_5 \sin\theta_5)^2 = (a_2 - a_3)^2 \quad (14)$$

Equation (10) can be converted into (15) and (16).

$$a_9 \cos(\pi - \eta) + a_5 \cos\theta_5 + a_7 \cos(\theta_4 - \beta) = S \cos\gamma + a_8 \cos\theta_8 \quad (15)$$

$$a_9 \sin(\pi - \eta) + a_5 \sin\theta_5 + a_7 \sin(\theta_4 - \beta) = S \sin\gamma + a_8 \sin\theta_8 \quad (16)$$

Equation (17) can be obtained by eliminating the variable S.

$$\frac{a_9 \cos(\pi - \eta) + a_5 \cos\theta_5 + a_7 \cos(\theta_4 - \beta) - a_8 \cos\theta_8}{\cos\gamma} = \frac{a_9 \sin(\pi - \eta) + a_5 \sin\theta_5 + a_7 sin(\theta_4 - \beta) - a_8 \sin\theta_8}{\sin\gamma} \quad (17)$$

With $\tan\frac{\theta_8}{2}$ designated as x_8, $\sin\theta_8$ equals $\frac{2x_8}{1+x_8^2}$; $\cos\theta_8$ equals $\frac{1-x_8^2}{1+x_8^2}$. Equation (17) is converted into (18), which can be seen as a quadratic equation.

$$A_8 x_8^2 + B_8 x_8 + C_8 = 0 \quad (18)$$

In (18),

$$A_8 = a_9 \sin(\pi - \eta - \gamma) + a_5 sin(\theta_5 - \gamma) + a_7 \sin(\theta_4 - \beta - \gamma) - a_8 \sin\gamma$$

$$B_8 = -2a_8 \cos\gamma$$

$C_8 = a_9 \sin(\pi - \eta - \gamma) + a_5 \sin(\theta_5 - \gamma) + a_7 \sin(\theta_4 - \beta - \gamma) + a_8 \sin\gamma$.

With A_8 not equalling 0, the discriminant of (18) is (19).

$$\Delta_8 = B_8^2 - 4A_8C_8 \geq 0 \quad (19)$$

Equation (19) can be converted into (20).

$$\Delta_8 = 4K_1K_2 \geq 0 \quad (20)$$

In (20)

$$K_1 = a_8 - a_9 \sin(\pi - \eta - \gamma) - a_5 \sin(\theta_5 - \gamma) - a_7 \sin(\theta_4 - \beta - \gamma) \quad (21)$$

$$K_2 = a_8 + a_9 \sin(\pi - \eta - \gamma) + a_5 \sin(\theta_5 - \gamma) + a_7 \sin(\theta_4 - \beta - \gamma) \quad (22)$$

The value of x_8 can be obtained via (23) and (24).

$$x_{8[1]} = \frac{-B_8 - \sqrt{\Delta}_8}{2A_8} \quad (23)$$

$$x_{8[2]} = \frac{-B_8 + \sqrt{\Delta}_8}{2A_8} \quad (24)$$

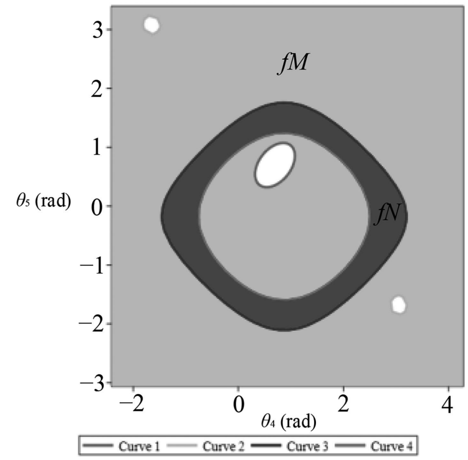

Figure 6. The branch graph of the planar two-DOF seven-bar mechanism with a prismatic pair without branch points.

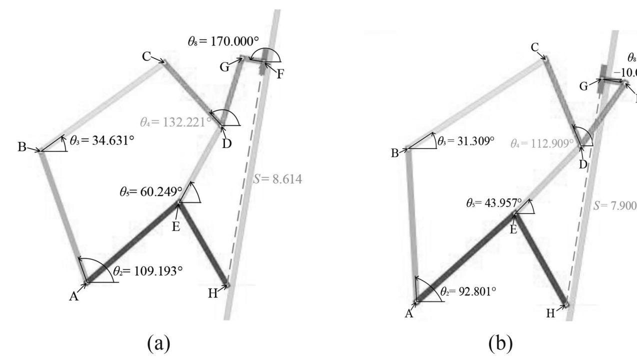

Figure 7. The 3D model of (a) the type-1 and (b) the type-2 singularity configurations.

3.2 Analysis of Branches

3.2.1 Analysis of Branches Without Branch Points

Table 3 enumerates the parameters for the two-DOF seven-bar mechanism with a prismatic pair without branch points.

Figure 6 shows the four singularity curves. Curves 1 to 4 are, respectively, obtained via (13), (14), (21)=0, and (22)=0. The light-shaded area, *fM*, is the JRS of ABCDE surrounded by curves 1 and 2. The dark-shaded area surrounded by curves 3 and 4, *fN*, is the JRS of HEDFG. Since *fM* completely covers *fN* and no branch points exist, the proposed mechanism's motion is only decided by *fN* and has decoupled motion. Therefore, the branch is *fN*; branch curves are curves 3 and 4. Joints A, B, and C can never be collinear. The mechanism can encounter two types of singularity configurations; the displacements of all joints in two singularity configurations, each of which belongs to a type of singularity configurations, are displayed in Table 4.

The type-one singularity configuration is shown in Fig. 7(a); the type-two singularity configuration is shown in Fig. 7(b).

Table 3
The Parameters for the Two-DOF Planar Seven-Bar Mechanism with a Prismatic Pair Without Branch Points

a_1	a_2	a_3	a_4		a_5	a_7	a_8	a_9	α	η	γ	β
4.69	5.30	5.85	3.25		3.35	2.69	0.85	3.65	40°	60°	80°	60°

Table 4
The Precise Displacements of All Joints in the Two Singularity Configurations

Joints	θ_2	θ_3	θ_4	θ_5	θ_8	S
Type-1	109.193°	34.631°	132.221°	60.249°	170.000°	8.614
Type-2	92.801°	31.309°	112.909°	43.957°	−10.000°	7.900

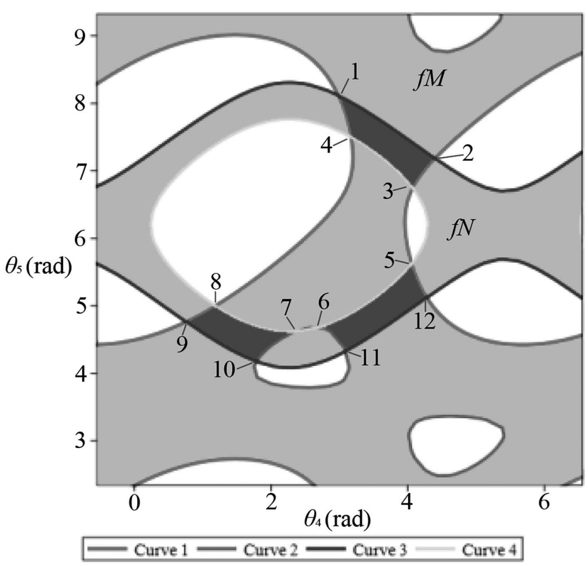

Figure 8. The branch graph of the planar two-DOF seven-bar mechanism with a prismatic pair with branch points.

In the type-1 and type-2 singularity configurations, the displacements of θ_4 and θ_5 are (132.221°, 60.249°) on curve 3 and (112.909°, 43.957°) on curve 4 shown in Fig. 6; θ_2 was acquired via (4) and θ_3 was acquired via (2) or (3); θ_8 was obtained via (23) or (24); S was acquired through (15) or (16). As per Table 4, when (21) or (22) equals 0, link FG is vertical to prismatic pair G_P, as is shown in Fig. 7.

3.2.2 Analysis of Branches with Branch Points

Table 5 lists the parameters for the planar two-DOF seven-bar mechanism with a prismatic pair with branch points.

Fig. 8 shows 4 singularity curves.

Curves 1 to 4 are, respectively, obtained via (13), (14), (21)=0, and (22)=0. The light-shaded area, *fM*, is the JRS of ABCDE. The light-shaded area surrounded by curves 3 and 4 is represented by *fN*, which is the JRS of HEDFG. The three dark-shaded shared areas of *fM* and *fN* are the branches; the mechanism has coupled motion. The intersection points of the 4 curves are called branch points obtained via (13), (14), (21)=0, and (22)=0. There are 12 branch points shown in Table 6.

At each branch point, passive joints A, B, and C are collinear. Since all 12 branch points are on either curve 3 or 4, Δ_8 equals 0 at each branch point. Each joint's displacement at branch points can be obtained, which is shown in Table 7. The displacement of θ_2 was acquired via (11) or (12) and the displacement of θ_8 was obtained via (23) or (24). Finally, S was obtained through (15) or (16).

Note: If S is a positive value, prismatic pair G_P is above AH in Fig. 4(a). If S is a negative value, G_P is below AH.

The 3D model of the proposed mechanism simulated the mechanism's motion and verified each joint's displacement at each branch point. The mechanism's singularity configurations at branch points are shown in Fig. 9.

As per Fig. 9, link FG is vertical to prismatic pair G_P at each branch point.

3.3 Identification of Sub-branches

If the proposed mechanism transforms between two different sub-branches, it will encounter singularity configurations where μ_1 in Fig. 4(a) equals 0° or 180° and μ_2 in Fig. 4(a) equals 90° or 270°. A branch has at most four sub-branches according to whether $\mu_1 \in (0°, 180°)$ or $(180°, 360°)$, and whether $\mu_2 \in (-90°, 90°)$ or $(90°, 270°)$. With a set of given values for θ_4 and θ_5, P, sub-branches of the proposed mechanism with branch points were identified. The results are shown in Table 8.

Note: When S has a positive value, prismatic pair G_P is above AH in Fig. 4(a). When S has a negative value, prismatic pair G_P is below AH.

The 3D model of the proposed mechanism also verified the displacement of the mechanism's each joint at each set of input values. The four configurations of the proposed mechanism at the given set of input values are shown in Fig. 10.

P is in the branch that has 5th, 6th, 11th, and, 12th branch points in Fig. 8. The first sub-branch, where μ_1 is within 0° to 180°, contains, $P_{[3]}$ and $P_{[4]}$. The second sub-branch, where μ_1 is within 180° to 360°, contains, $P_{[1]}$ and $P_{[2]}$. The third sub-branch, where μ_2 is within −90° to 90°, contains $P_{[1]}$ and $P_{[3]}$.The fourth sub-branch, where μ_2 is within 90° to 270°, contains $P_{[2]}$ and $P_{[4]}$.

Table 5
The Parameters for the Two-DOF Planar Seven-Bar Mechanism with a Prismatic Pair with Branch Points

a_1	a_2	a_3	a_4	a_5	a_7	a_8	a_9	α	η	γ	β
3.69	3.30	1.85	2.25	3.35	2.33	0.85	3.45	25°	70°	85°	135°

Table 6
The 12 Branch Points in Fig. 8(a)

	1	2	3	4	5	6	7	8	9	10	11	12
θ_4	171.068°	251.955°	233.383°	181.800°	232.471°	153.939°	135.506°	67.897°	43.597°	102.282°	177.271°	245.047°
θ_5	465.052°	411.660°	386.794°	429.998°	322.051°	268.054°	264.808°	286.318°	272.924°	239.256°	248.116°	293.422°

Table 7
The Displacement of the Joints in the Two-DOF Planar Seven-Bar Mechanism with a Prismatic Pair at Branch Points

Joints	θ_2	θ_3	θ_4	θ_5	θ_8	S
1	87.200°	87.200°	171.068°	465.052°	175.000°	7.804
2	23.429°	23.429°	251.955°	411.660°	175.000°	7.902
3	14.203°	14.203°	233.383°	386.794°	−5.000°	7.158
4	64.203°	64.203°	181.800°	429.998°	−5.000°	8.194
5	−26.339°	−26.339°	232.471°	322.051°	−5.000°	3.580
6	−33.490°	146.510°	153.939°	268.054°	−5.000°	0.727
7	−7.925°	172.075°	135.506°	264.808°	−5.000°	0.0003
8	4.779°	4.779°	67.897°	286.318°	−5.000°	−2.053
9	−2.611°	−2.611°	43.597°	272.924°	175.000°	−2.517
10	37.291°	217.291°	102.282°	239.256°	175.000°	−0.975
11	−96.009°	83.991°	177.271°	248.116°	175.000°	1.633
12	−43.645°	−43.645°	245.047°	293.422°	175.000°	2.291

Table 8
The Identification of Sub-branches of the Two-DOF Planar Seven-Bar Mechanism with a Prismatic Pair

Joints	(θ_4, θ_5)	θ_2	θ_3	μ_1	θ_8	S	μ_2
$P_{[1]}$	(217.724°, 297.938°)	−66.750°	7.964°	254.714°	−62.567°	3.361	−32.433°
$P_{[2]}$	(217.724°, 297.938°)	−66.750°	7.964°	254.714°	52.540°	1.926	212.460°
$P_{[3]}$	(217.724°, 297.938°)	−16.329°	−88.980°	107.349°	−62.567°	3.361	−32.433°
$P_{[4]}$	(217.724°, 297.938°)	−16.329°	−88.980°	107.349°	52.540°	1.926	212.460°

4. Kinematic Analysis of the Planar Two-DOF Seven-Bar Mechanism with Two Prismatic Pairs

4.1 The Establishment of the Euler Loop Equation Based on Euler's Formula

Figure 11(a) shows the schematic diagram of the planar two-DOF seven-bar mechanism with two prismatic pairs. Figure 11(b) shows the 3D model of the mechanism.

In Fig. 11, prismatic pair B_P and revolute pair B_R are all on slider B; prismatic pair G_P and revolute pair G_R are all on the slider G. Other revolute pairs include C, D, E, and F. a_i represents the length of a specific link or a specific side of a link and θ_i represents the displacement of a specific joint. The sides, AE and EH, of the triangular link AEH are at ψ and η degrees with the horizontal line, respectively. The angle that is formed by the two sides, CD and DF, of the triangular link CDF is β. The translational

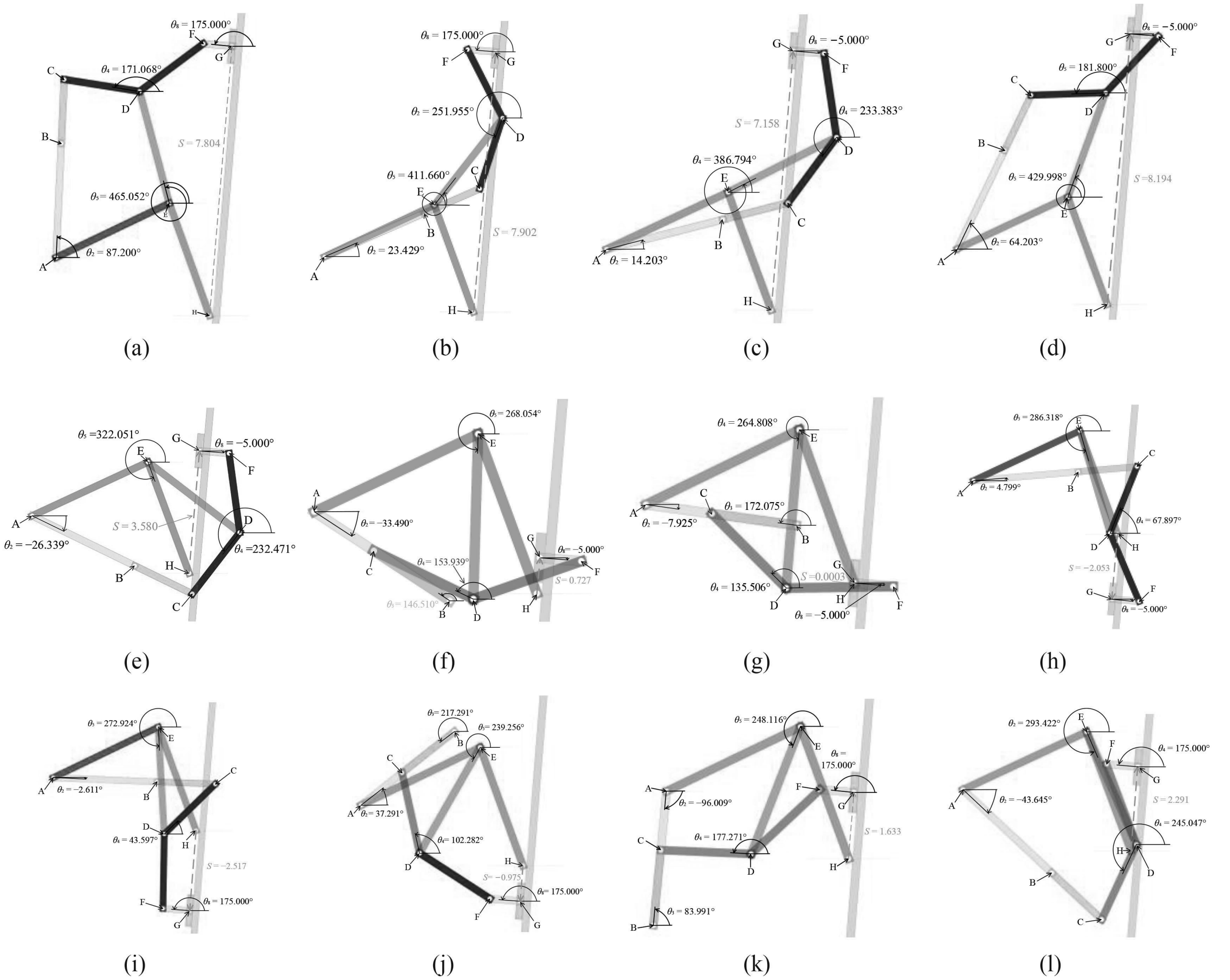

Figure 9. The singularity configurations of the two-DOF seven-bar planar mechanism with a prismatic pair at each branch point: (a) branch point 1; (b) branch point 2; (c) branch point 3; (d) branch point 4; (e) branch point 5; (f) branch point 6; (g) branch point 7; (h) branch point 8; (i) branch point 9; (j) branch point 10; (k) branch point 11; (l) branch point 12.

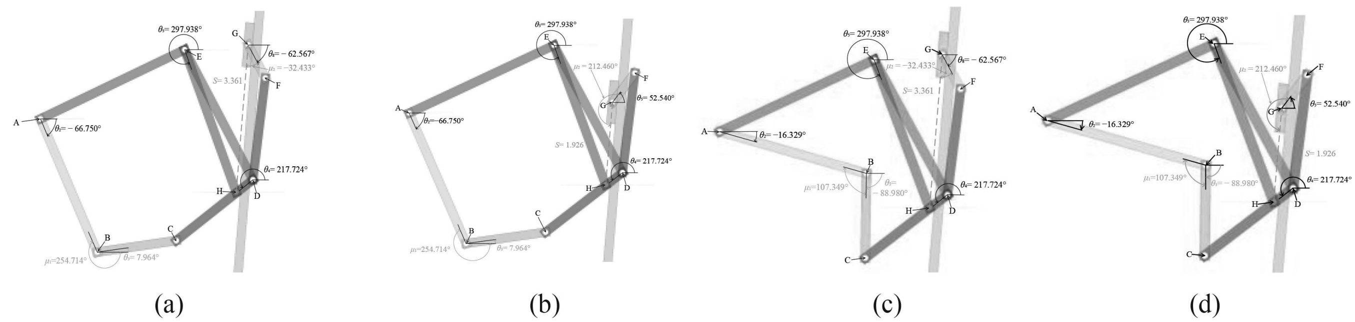

Figure 10. The configurations of the two-DOF planar seven-bar mechanism with a prismatic pair at the given set of input values: (a) $P_{[1]}$; (b) $P_{[2]}$; (c) $P_{[3]}$; (4) $P_{[4]}$.

displacements of sliders B and G are represented by S_1 and S_2, respectively. Each solid line with an arrow is a link or a side of a link in the mechanism represented by a vector; the two dotted lines with an arrow $\overrightarrow{AB}$ and $\overrightarrow{HG}$ are also vectors that represent the translational motion created by B and G respectively; $\overrightarrow{AB}$ and $\overrightarrow{HG}$ are at an angle of α_1 and α_2 degrees with the horizontal line, respectively. With θ_3 and θ_4 being the input angles and link AEH being the fixed link, the Euler loop equations based on Euler's formula for the two five-bar kinematic chains in the mechanism are established. In the five-bar kinematic chain ABCDE, since $\overrightarrow{AB} + \overrightarrow{BC} = \overrightarrow{AE} + \overrightarrow{ED} + \overrightarrow{DC}$, (25) can be obtained.

$$S_1 e^{i\alpha_1} + a_2 e^{i\theta_2} = a_1 e^{i\psi} + a_4 e^{i\theta_4} + a_3 e^{i\theta_3} \tag{25}$$

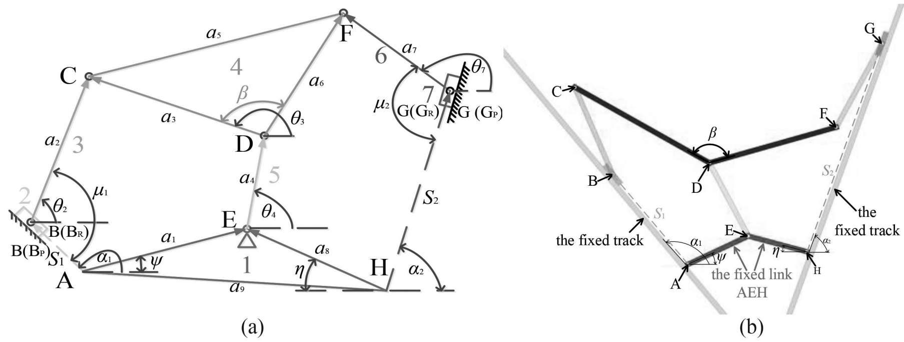

Figure 11. (a) The schematic diagram; (b) the 3D model of the planar two-DOF seven-bar mechanism with two prismatic pairs.

In the five-bar kinematic chain HEDFG, $\overrightarrow{\mathrm{HE}}+\overrightarrow{\mathrm{ED}}+\overrightarrow{\mathrm{DF}}=\overrightarrow{\mathrm{HG}}+\overrightarrow{\mathrm{GF}}$, (26) can be derived.

$$a_8e^{i(\pi-\eta)}+a_4e^{i\theta_4}+a_6e^{i(\theta_3-\beta)}=S_2e^{i\alpha_2}+a_7e^{i\theta_7} \quad (26)$$

To analyse ABCDE, (25) is converted into (27) and (28).

$$S_1\cos\alpha_1+a_2\cos\theta_2 = a_1\cos\psi+a_4\cos\theta_4+a_3\cos\theta_3 \quad (27)$$

$$S_1\sin\alpha_1+a_2\sin\theta_2 = a_1\sin\psi+a_4\sin\theta_4+a_3\sin\theta_3 \quad (28)$$

By eliminating S_1, (29) is established.

$$\frac{a_1\cos\psi+a_4\cos\theta_4+a_3\cos\theta_3-a_2\cos\theta_2}{\cos\alpha_1} = \frac{a_1\sin\psi+a_4\sin\theta_4+a_3\sin\theta_3-a_2\sin\theta_2}{\sin\alpha_1} \quad (29)$$

With x_2 designated as $\tan\frac{\theta_2}{2}$, $\sin\theta_2$ equals $\frac{2x_2}{1+x_2^2}$ and $\cos\theta_2$ equals $\frac{1-x_2^2}{1+x_2^2}$. (29) can be converted into (30), which can be seen as a quadratic equation.

$$A_2x_2^2+B_2x_2+C_2=0 \quad (30)$$

In (30),

$$\begin{aligned} A_2 &= a_1\sin(\psi-\alpha_1)+a_4\sin(\theta_4-\alpha_1) \\ &\quad +a_3\sin(\theta_3-\alpha_1)-a_2\sin\alpha_1 \\ B_2 &= -2a_2\cos\alpha_1 \end{aligned}$$

$C_2=a_1 sin(\psi-\alpha_1)+a_4 sin(\theta_4-\alpha_1)+a_3 sin(\theta_3-\alpha_1)+a_2\sin\alpha_1$.

When A_2 does not equal 0, (31) is the discriminant of (30).

$$\Delta_2=B_2^2-4A_2C_2\geq 0 \quad (31)$$

Equation (31) can be converted in (32).

$$\Delta_2=4R_1R_2\geq 0 \quad (32)$$

In (32),

$$\begin{aligned} R_1 &= a_2-a_1\sin(\psi-\alpha_1)-a_4\sin(\theta_4-\alpha_1) \\ &\quad -a_3\sin(\theta_3-\alpha_1) \quad (33) \\ R_2 &= a_2+a_1\sin(\psi-\alpha_1)+a_4\sin(\theta_4-\alpha_1) \\ &\quad +a_3\sin(\theta_3-\alpha_1). \quad (34) \end{aligned}$$

The exact values of x_2 can be obtained via (35) and (36).

$$x_{2[1]} = \frac{-B_2-\sqrt{\Delta_2}}{2A_2} \quad (35)$$

$$x_{2[2]} = \frac{-B_2+\sqrt{\Delta_2}}{2A_2} \quad (36)$$

To analyse HEDFG, (26) is converted into (37) and (38).

$$\begin{aligned} & a_8\cos(\pi-\eta)+a_4\cos\theta_4+a_6\cos(\theta_3-\beta) \\ & \quad = S_2\cos\alpha_2+a_7\cos\theta_7 \quad (37) \\ & a_8\sin(\pi-\eta)+a_4\sin\theta_4+a_6\sin(\theta_3-\beta) \\ & \quad = S_2\sin\alpha_2+a_7\sin\theta_7 \quad (38) \end{aligned}$$

By eliminating S_2, (39) is established.

$$\frac{a_8 cos(\pi-\eta)+a_4\cos\theta_4+a_6 cos(\theta_3-\beta)-a_7\cos\theta_7}{\cos\alpha_2} = \frac{a_8 sin(\pi-\eta)+a_4\sin\theta_4+a_6 sin(\theta_3-\beta)-a_7\sin\theta_7}{\sin\alpha_2}=S_2 \quad (39)$$

With x_7 designated as $\tan\frac{\theta_7}{2}$, $\sin\theta_7$ equals $\frac{2x_7}{1+x_7^2}$ and $\cos\theta_7$ equals $\frac{1-x_7^2}{1+x_7^2}$; (39) can be converted into (40), which can also be seen as a quadratic equation.

$$A_7x_7^2+B_7x_7+C_7=0 \quad (40)$$

In (40),

$$\begin{aligned} A_7 &= a_8\sin(\pi-\eta-\alpha_2)+a_4\sin(\theta_4-\alpha_2) \\ &\quad +a_6\sin(\theta_3-\beta-\alpha_2)-a_7\sin\alpha_2 \\ B_7 &= -2a_7\cos\alpha_2 \end{aligned}$$

$C_7=a_8\sin(\pi-\eta-\alpha_2)+a_4\sin(\theta_4-\alpha_2)+a_6\sin(\theta_3-\beta-\alpha_2)+a_7\sin\alpha_2$.

When A_7 does not equal 0, (41) is the discriminant of (40).

$$\Delta_7=B_7^2-4A_7C_7\geq 0 \quad (41)$$

Table 9
The Parameters for the Two-DOF Seven-Bar Mechanism with Two Prismatic Pairs with Branch Points

a_1	a_2	a_3	a_4	a_6	a_7	a_8	α_1	α_2	ψ	η	β
2.69	3.85	6.25	3.35	5.33	3.85	2.45	130°	70°	25°	15°	135°

Table 10
The Four Branch Points in Fig. 12

Branch points	1	2	3	4
θ_3	149.515°	97.534°	248.903°	183.807°
θ_4	395.470°	271.108°	293.047°	154.785°

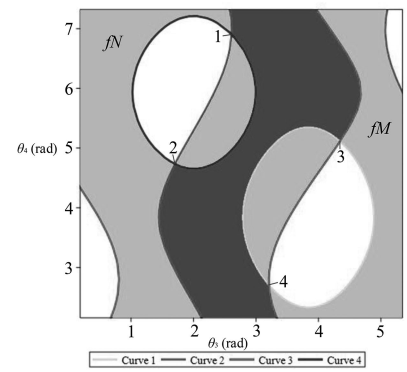

Figure 12. The branch graph and the 3D model of the planar two-DOF seven-bar mechanism with two prismatic pairs with branch points.

Equation (41) can be converted into (42).

$$\Delta_7 = 4Q_1Q_2 \geq 0 \quad (42)$$

In (42),

$$\begin{aligned} Q_1 &= a_7 - a_8\sin(\pi - \eta - \alpha_2) - a_4\sin(\theta_4 - \alpha_2) \\ &\quad -a_6\sin(\theta_3 - \beta - \alpha_2) \quad (43) \\ Q_2 &= a_7 + a_8\sin(\pi - \eta - \alpha_2) + a_4\sin(\theta_4 - \alpha_2) \\ &\quad +a_6\sin(\theta_3 - \beta - \alpha_2). \quad (44) \end{aligned}$$

The exact values of x_7 can be obtained via (45) and (46).

$$x_{7[1]} = \frac{-B_7 - \sqrt{\Delta_7}}{2A_7} \quad (45)$$

$$x_{7[2]} = \frac{-B_7 + \sqrt{\Delta_7}}{2A_7} \quad (46)$$

4.2 The Analysis of Branches

Table 9 enumerates the parameters for the mechanism with branch points.

Figure 12 shows the branch and branch points of the proposed mechanism.

Curves 1 to 4 are, respectively, obtained via (33)=0, (34)=0, (43)=0, and (44)=0. The light-shaded area surrounded by curves 1 and 2, *fM*, is the JRS of ABCDE. The light-shaded area surrounded by curves 3 and 4, *fN*, is the JRS of HEDFG. The dark-shaded shared section of *fM* and *fN* is the branch of the mechanism. The branch points can be identified via (33)=0, (34)=0, (43)=0 and (44)=0, respectively. There are four branch points shown in Table 10.

At each branch point, both Δ_2 and Δ_7 equal 0. The displacements of other joints can be obtained and are shown in Table 11.

Note: if S_1 has a negative value, prismatic pair B_P is below AH in Fig. 11(a). If S_1 has a positive value, B_P is above AH. If S_2 has a negative value, prismatic pair G_P is below AH. If S_2 has a positive value, G_P is above AH.

Equations (35) and (36) were utilised to obtain θ_2; (27) and (28) were employed to acquire S_1; (45) and (46) were used to obtain θ_7; (37) and (38) were deployed to obtain S_2. According to Table 11, at each branch point, links BC and FG are, respectively, vertical to prismatic pairs B_P and G_p. The 3D model of the proposed mechanism simulated the mechanism's singularity configurations at branch points, which are shown in Fig. 13.

4.3 Analysis of Sub-branches

With a set of given values for θ_3 and θ_4, P, the sub-branches of the proposed mechanism with parameters in Table 10 were identified. The results are in Table 12.

Note: if S_1 has a negative value, prismatic pair B_P is below AH in Fig. 11(a). If S_1 has a positive value, B_P is above AH. If S_2 has a negative value, prismatic pair G_P is below AH. If S_2 has a positive value, G_P is above AH.

Figure 14 enumerates the four configurations of the mechanism at the given set of input values, which were simulated and verified by the 3D model of the mechanism.

The first sub-branch, where μ_1 is within $-90°$ to $90°$, contains $P_{[1]}$ and $P_{[3]}$. The second sub-branch, where μ_1 is within $90°$ to $270°$, contains $P_{[2]}$ and $P_{[4]}$. The third sub-branch, where μ_2 is within $-90°$ to $90°$, contains $P_{[3]}$ and $P_{[2]}$. The fourth sub-branch, where μ_2 is within $90°$ to $270°$, contains $P_{[3]}$ and $P_{[4]}$.

Table 11
The Displacement of the Joints in the Planar Two-DOF Seven-Bar Mechanism with Two Prismatic Pairs at Branch Points

Branch Points	S_1	θ_2	θ_3	θ_4	θ_7	S_2
1	4.930	40.000°	149.515°	395.470°	−20.000°	5.566
2	1.970	40.000°	97.534°	271.108°	−20.000°	−4.938
3	−6.921	−140.000°	248.903°	293.047°	160.000°	1.179
4	6.036	−140.000°	183.807°	154.785°	160.000°	5.061

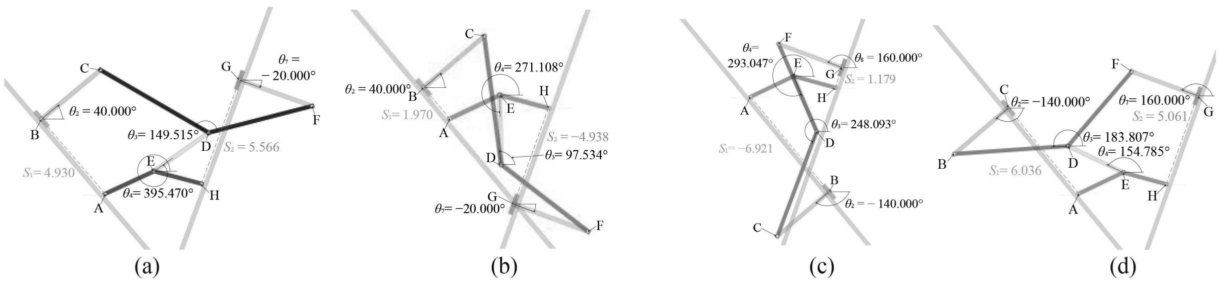

Figure 13. The singularity configurations of the two-DOF planar seven-bar mechanism with two prismatic pairs at each branch point: (a) branch point 1; (b) branch point 2; (c) branch point 3; and (4) branch point 4.

Table 12
The Identification of Sub-Branches of the Planar Two-DOF Seven-Bar Mechanism with Two Prismatic Pairs

Positions	(θ_3, θ_4)	θ_2	S_1	μ_1	θ_7	S_2	μ_2
$P_{[1]}$	(143.239°, 171.887°)	−66.119°	11.580	−16.119°	−125.420°	5.330	15.420°
$P_{[2]}$	(143.239°, 171.887°)	146.104°	4.183	196.104°	−125.420°	5.330	15.420°
$P_{[3]}$	(143.239°, 171.887°)	−66.119°	11.580	−16.119°	85.428°	−2.093	164.572°
$P_{[4]}$	(143.239°, 171.887°)	146.104°	4.183	196.104°	85.428°	−2.093	164.572°

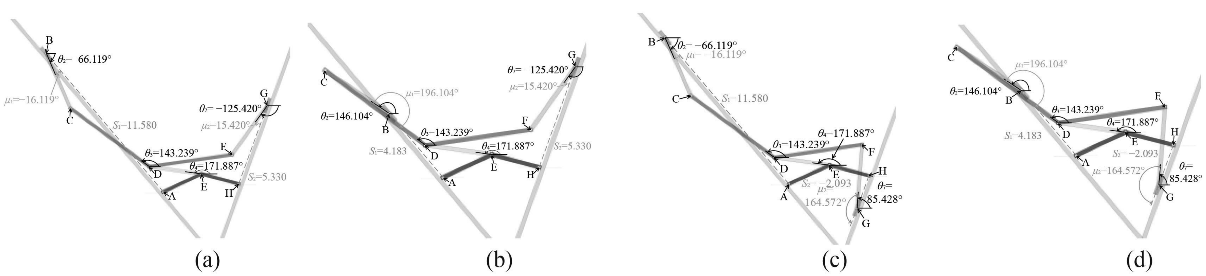

Figure 14. Configurations of the two-DOF seven-bar planar mechanism with two prismatic pairs at the given set of input values: (a) $P_{[1]}$; (b) $P_{[2]}$; (c) $P_{[3]}$; and (d) $P_{[4]}$.

5. Conclusions and Discussion

This paper extends research on planar complex mechanisms with only revolute pairs to the research on planar complex mechanisms with not only revolute pairs but also prismatic pairs. Proposed in this paper are the two-DOF planar seven-bar mechanisms with a prismatic pair and two prismatic pairs to produce translational output movement. On the basis of the rotatability laws for N-bar kinematic chains, the concept of JRS, and the discriminant method, the motion characteristics of the two proposed mechanisms were systematically analysed via the kinematic analysis methodology proposed in this paper. The kinematic analysis methodology successfully identified and verified the branches, branch points, and sub-branches of the two proposed mechanisms; the method also accurately obtained and verified the displacements of revolute and prismatic joints of the two proposed mechanisms at branch points and in sub-branches.

However, the study into planar multi-loop mechanisms needs to be more thorough. Prismatic pairs can be introduced into single-DOF planar eight-bar mechanisms and three-DOF planar eight-bar mechanisms to create translational motion. Prismatic pairs can also be employed in two-DOF spherical seven-bar mechanisms to diversify their motion. Future research should focus on those mechanisms with prismatic pairs.

References

[1] K.-L. Ting, Five-bar Grashof criteria, *ASME Journal of Mechanisms, Transmissions, and Automation in Design, 108*(4), 1986, 533–537.

[2] K.-L. Ting, Mobility criteria of single-loop N-bar linkages, *Journal of Mechanisms, Transmissions, and Automation in Design, 111*(4), 1989, 504–507.

[3] K.-L. Ting and Y.-W. Liu, Rotatability laws for N-bar kinematic chains and their proof, *Journal of Mechanism Design, 113*(1), 1991, 32–39.

[4] Y.-W. Liu and K.-L. Ting, On the rotatability of spherical N-bar chains, *Journal of Mechanical Design, 116*(3), 1994, 920–923.

[5] K.-L. Ting, On the input joint rotation space and mobility of linkages, *Journal of Mechanical Design, 130*(9), 2008, 1–12.

[6] K.-L. Ting and X. Dou, Classification and branch identification of Stephenson six-bar chains, *Mechanism and Machine Theory, 31*(3), 1996, 283–295.

[7] K.-L. Ting, C. Xue, J. Wang, and K.R. Currie, Stretch rotation and complete mobility identification of Watt six-bar linkages, *Mechanism and Machine Theory, 44*(10), 2009, 1877–1886.

[8] K.-L. Ting, J. Wang, C. Xue, and K.R. Currie, Full rotatability and singularity of six-bar and geared five-bar linkages, *Journal of Mechanisms and Robotics-Transactions of the ASME*, *2*(1), 2010, 298–300.

[9] X. Dou and K.-L. Ting, Module approach for branch analysis of multiloop linkages/manipulators, *Mechanism and Machine Theory, 33*(5), 1998, 565–582.

[10] J. Wang, K.-L. Ting, and C. Xue, Discriminant method for the mobility identification of single degree-of-freedom double-loop linkages, *Mechanism and Machine Theory, 4*(5), 2010, 740–755.

[11] J. Wang, K.-L. Ting, and D. Zhao, Equivalent linkages and dead center positions of planar single-degree-of-freedom complex linkages, *Journal of Mechanisms and Robotics-Transactions of the ASME, 7*(4), 2015, 044501.

[12] J. Wang and K.-L. Ting, Mobility identification of a group of single degree-of-freedom eight-bar linkages, *Proc. of the ASME 2010 International Design Engineering Technical Conf. and Computers and Information in Engineering Conf.,* Montreal, QC, 2010, 1739–1749.

[13] M. M. Plecnik and J.M. McCarthy, Kinematic synthesis of Stephenson III six-bar function generators, *Mechanism and Machine Theory, 97*(9), 2016, 112–126.

[14] J. Wang, K.-L. Ting, C. Xue, and K.R. Currie, Singularity and sub-branch identification of two-DOF seven-bar parallel manipulators, *Proc. of the ASME 2009 International Design Engineering Technical Conf. and Computers and Information in Engineering Conf.*, San Diego, CA, 2009, 1139–1146.

[15] J. Wang, K.-L. Ting, and C. Xue, Branch identification of planar two-DOF seven-bar linkages, *Proc. of the ASME 2009 International Design Engineering Technical Conf. and Computers and Information in Engineering Conf.*, San Diego, CA, 2009, 1175–1182.

[16] J. Wang, K.-L. Ting, Y. Gong, and H. He, Motion continuity and branch identification of two-DOF seven-bar planar parallel manipulators and linkages, *International Journal of Robotics and Automation, 34*(4), 2019, 397–409.

[17] J. Wang, L. Nie, D. Zhao, J. Ren, Q. Wang, J. Sun, and K.-L. Ting, Equivalent five-bar linkages for the singularity analysis of two-DOF seven-bar linkages, *Proc. of International Design Engineering Technical Conf. and Computer and Information in Engineering Conf.*, Cleveland, OH, 2017.

[18] L. Nie and H, Ding, Dead center identification of two-degrees-of-freedom planar parallel manipulator using graph theory and transmission angle, *Journal of Mechanisms and Robotics-Transactions of the ASME, 12*(5), 2022, 1–15.

[19] J. Wang, L. Nie, Q. Wang, J. Sun, Y. You, D. Zhao, K.-L. Ting, Singularity analysis of planar multiple-DOF linkages, *Proc. of the ASME 2014 International Design Engineering Technical Conf. and Computers and Information in Engineering Conf.*, Buffalo, NY, 2014.

[20] W. Liu, J. Han, and L. Qiu, On the theory and methodology of systematic analysis of positions, singular configurations, branches and circuits, and ranges of motion for planar complex linkages, *Mechanism and Machine Theory, 168*, 2022, 104590.

[21] C.L. Chan and K.-L. Ting, Rotatability of the floating link on multi-loop planar linkages, *Journal of Mechanisms and Robotics-Transactions of the ASME, 12*(6), 2020, 061007.

[22] Q. Zhao, J. Guo, and J. Hong, Assembly precision prediction for planar closed-loop mechanism in view of joint clearance and redundant constraint, *Journal of Mechanical Science and Technology, 32*(7), 2018, 3395–3405.

[23] J. Ding, S, Lyu, T. Da, C. Wang, and G.S. Chirikjian, Error space estimation of three degrees of freedom planar parallel mechanisms, *Journal of Mechanisms and Robotics-Transactions of the ASME, 11*(3), 2019, 031013.

[24] D. Yao, Y. Wu, Y. Wang, and X. Xiao, Experimental validation of a control method for underactuated bipedal walking on compliant ground, *International Journal of Robotics and Automation, 33*(5), 2018, 552–558.

[25] X. Lai, H. Chen, Y. Wang, Y. Yuan, and M. Wu, Trajectory tracking control with specified posture for planar four-link real underactuated manipulator, *International Journal of Robotics and Automation, 34*(2), 2019, 194–202.

[26] K. Marlow, M. Isaksson, and S. Nahavandi, Motion/force transmission analysis of planar parallel mechanisms with closed-loop subchains, *Journal of Mechanisms and Robotics-Transactions of the ASME, 8*(4), 2016, 041019.

[27] N. Robson and S. Ghosh, Geometric design of planar mechanisms based on virtual guides for manipulation, *Robotica, 34*(12), 2016, 2653–2668.

[28] Z. Yang and D. Zhang, Novel planar balanced (2-RR)R parallel manipulator adaptive for energy efficiency, *International journal of Robotics and Automation, 35*(6), 2020, 454–459.

[29] Z. Shao, H. Li, L. Wang, Z. Zhang, R. Yao, and J. Qie, Orientation optimization of cable-driven parallel manipulator for cleaning the deep sea fishing ground, *International Journal of Robotics and Automation, 35*(5), 2020, 347–354.

[30] Z. Zhan, X. Zhang, Z.C. Jian, and H.D. Zhang, Error modelling and motion reliability analysis parallel manipulator with multiple uncertainties, *Mechanism and Machine Theory, 124*, 2018, 55–72

[31] G. Chen, Z. Zhang, L. Kong, and H. Wang, Analysis and validation of a flexible planar two degrees-of-freedom parallel manipulator with structural passive compliance, *Journal of Mechanisms and Robotics-Transaction of the ASME, 12*(1), 2020, 011011.

[32] K. Li, H. Jiang, and Z. Cui, Design for solving negative stiffness problem of redundant planar rotational parallel mechanisms, *International Journal of Robotics and Automation, 34*(1), 2019, 78–83.

[33] G. Chen, J. Wang, and W. Hao, A new type of planar two degrees-of-freedom remote center-of-motion mechanism inspired by the peaucellier-lipkin straight-line linkage, *Journal of Mechanical Design, 141*(1), 2019, 015001.

[34] G.S. Soh and F.T. Ying, Motion generation of planar six- and eight-bar slider mechanisms as constrained robotic systems, *Journal of Mechanisms and Robotics-Transactions of the ASME, 7*(3), 2015, 975–978.

[35] S.M. Almestiri, A.P. Murray, D.H. Myszka, and C.W. Wampler, Singularity traces of single degree-of-freedom planar linkages that include prismatic and revolute joints, *Journal of Mechanisms and Robotics-Transactions of the ASME, 8*(5), 2015, 15–18.

[36] Q, Zou, D. Zhang, S, Zhang, and X. Luo, Kinematic and dynamic analysis of a 3-DOF parallel mechanism, *International*

Journal of Mechanics and Materials in Design, 17*(3), 2021, 587–599.

[37] S. Zarkandi, An instant center approach for isotropy analysis of planar parallel mechanisms, *International Journal of Robotics and Automation, 31*(5), 2016, 396–401.

[38] M. Helal, J, Hu, and H. Eleashy, Automatic generation of N-bar planar linkages containing sliders, *Applied Sciences-Basel, 11*(8), 2021, 3546.

[39] V. Dharanipragada and M. Chintada, Split hamming string as an isomorphism test for one degree-of-freedom planar simple-jointed kinematic chains containing Sliders, *Journal of Mechanical Design, 138*(8), 2016, 082301.

[40] S.W. Kang and Y.Y. Kim, Unified topology and joint types optimization of general planar linkage mechanisms, *Structure and Multidisciplinary of optimization, 57*(5), 2018, 1955–1983.

[41] J.S. Zhao, S. Wei, and J. Ji, Kinematic of a planar slider-crank in screw form, *Proceedings of the Institution of Mechanical Engineers Part C-Journal of Mechanical Engineering Science, 236*(3), 2022, 1588–1597.

[42] T. Essomba and S.N. Phu, Kinematic design of a hybrid-tripod mechanism for bone reduction surgery, *Mechanics and Industry, 21*(4), 2022, 403.

[43] M. Gallant and C. Gosselin, Singularities of a planar 3-RPR parallel manipulator with joint clearance, *Robotica, 36*(7), 2018, 1098–1109.

[44] C.S. Jhuang, Y.Y. Kao, and D.Z. Chen, Design of one DOF closed-loop statically balanced planar linkage with link-collinear spring arrangement, *Mechanism and Machine Theory, 130*, 2018, 301–312.

[45] S.J. Rodríguez-González, H.A. Suárez-Velásquez, J. Jesús Cervantes-Sánchez, and J.M. Rico-Martínez, A novel approach for the rigid body guidance synthesis of planar RRPR linkages, *Journal of Mechanical Science and Technology, 34*(2), 2020, 843–854.

Biographies

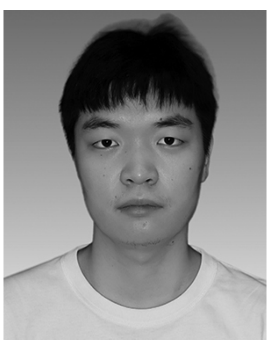

Mingquan Yang received the B.E. degree in mechanical design, manufacturing, and automation from Wuhan Donghu University, Wuhan, Hubei Province, Peoples Republic of China, in June 2018, and the masters degree in mechanical engineering from Hubei University of Technology, Wuhan, Hubei Province, Peoples Republic of China, in June 2023. His research topics include multi-loop planar and spherical mechanisms, industrial robotics, and additive manufacturing.

Jun Wang received the B.S. degree in aircraft design from Beijing University of Aeronautics and Astronautics in 2002, and the M.S. and Ph.D. degrees in mechanical engineering from Tennessee Technological University, Cookeville, TN, USA, in 2007 and 2010, respectively. He is currently a Professor with the School of Mechanical Engineering, Hubei University of Technology, Wuhan, Hubei Province, Peoples Republic of China. He is the author of more than 50 journal articles and holds more than 100 patents. His research interests include mechanisms, robotics, advanced manufacturing, renewable energy, mechanical design and theory, 3D printing, electromechanical controlling techniques, and intelligent manufacturing with human–robot cooperation. He is a peer reviewer of *Journal of Mechanical Design*, *Journal of Mechanisms and Robotics*, and *Mechanism and Machine Theory*. He was the recipient of the ASME A.T. Yang Academic Award for his outstanding achievements in robotic mechanisms in 2009.

Yizhe Huang received the Ph.D. degree in mechanical engineering from Huazhong University of Science and Technology, Wuhan, Hubei Province, Peoples Republic of China, in 2021. He is currently a Lecturer with the School of Mechanical Engineering, Hubei University of Technology, Wuhan, Hubei Province, Peoples Republic of China. He possesses more than 10 patents and has authored more than 30 journal articles. His primary areas of interest in research include robotics, intelligent manufacturing using human–machine collaboration, advanced manufacturing, noise and vibration control, and electromechanical control technologies. He serves as a peer reviewer for the *Equipment Manufacturing Technology Journal*.